

# Dynamic design optimization of turbine-compressor unit by Ocvirk and Dubois elastohydrodynamic equations and Craig-Bampton approach

Diego Acerbo  
HSE at Bonatti S.p.A.  
Via Nobel, 2 A , 43122 Parma (Italy)  
email: diego.acerbo@bonatti.it

**Abstract**—This paper presents the results obtained analysing the dynamic behaviour and natural vibration modes of the components of a turbine-compressor unit, connected by toothed coupling. The study was undertaken with the aim of improving the dynamic behaviour of the system, identifying some critical characteristics, mainly linked to problems of misalignment which lead to elevated vibration levels in some bearings and to the rupture of the lubrication film. An accurate 3D parametric virtual model of the system was used, integrating FEM and Multibody calculation programmes to perform a dynamic analysis of the various components considered as deformable bodies. Information regarding some characteristics significant for the dynamics of the system was obtained in experimental trials, allowing the validation of the numerical models. In particular, the contact of the teeth of the turbine and compressor hubs with the teeth of the coupling bell were simulated, as well as the hydrodynamic effect of the lubrication in the shaft bearings. The analysis of the results highlighted the need to use models with deformable elements, and allowed the determination of the limiting conditions of misalignment.

**Index Terms**—3D Flexible modeling, Computational dynamic analysis, misalignmen, bearings, lubrication film.

## I. INTRODUCTION

Management of a modern petrochemical plant, where the sound functioning of the machines installed guarantees the reliability and continuity of production, must include continuous monitoring by means of dedicated systems. Checking for vibration is essential in verifying the correct functioning of mechanical systems and will evidence possible anomalies at their incipient stage [1], [2], [3], [4], [5], [6], [7]. The present study examines a steam turbine driving a centrifuge compressor installed in an ethylene refrigeration cycle, part of the thermal cracking unit at the Enichem plant at Priolo (Sicily). Lately, different tools and methodologies have been employed to study this typology of machinery [8], [9]. A multibody model, composed of flexible parts and developed with the ADAMS programme, was used to simulate the dynamic behaviour of the two rotors, turbine and compressor, linked by a toothed coupling. The model, validated by comparison with experimental data obtained using the monitoring system, was found to be particularly useful in the analysis of breakdowns, allowing the simulation of misalignment due to

TABLE I. TURBO-COMPRESSOR BEARING SPECIFICATIONS

Bearing	Int. Diam. [mm]	Ext. Diam. [mm]	Length [mm]	Type	Clearance [mm]
Compressor bearings	200	450	92	Michell radial, 5 sectors	0.24 +0.28 diametral
Turbine bearings	200	355	100	Michell radial, 5 sectors	0.3 +0.358 diametral
Compressor thrust bearing	165.1	317.5	50.8 (ring thickness)	Kingsbury 6 sectors ant.,6 post.	0.25 + 0.3 axial
Turbine thrust bearing	133.4	295.3	44.45 (ring thickness)	Kingsbury 6 sectors ant.,6 post.	0.18 +0.33 axial

jibbing of the coupling. The modeling methodology followed it is similar to that described by Cali et al. [10], [11].

The simplified Reynolds equations proposed by Ocvirk and Dubois [12] for short bearings were used to simulate the hydrodynamic reaction of the bearing on the pivot.

## II. TURBO-COMPRESSOR UNIT

The P2005A turbo-compressor in the ethylene production plant of Enichem Priolo is used to compress the mixture of hydrocarbon gases emitted at the head of the quench column. The machine, constructed by Nuovo Pignone, consists of three main parts: the steam driven turbine, the centrifuge compressor which compresses the gas, and the toothed coupling which transmits the torque from the turbine to the compressor. The axial turbine, delivers a maximum power of 20835 kW at 4190 rpm. The shaft rests on two radial hydrodynamic bearings of the Michell type (tilting pad bearings) and a hydrodynamic axial thrust bearing of the Kingsbury type. The steam and lubrication oil seals are secured by a series of rings cut on the rotor and mounted on the stator with a labyrinth system. The six-stages centrifuge compressor of horizontal open case type, with three intake flanges and one delivery flange positioned in the lower half-casing, again rests on two segmented hydrodynamic bearings and a Kingsbury-type thrust bearing (Tab. I).

The Maag toothed coupling, Zud8 type, in AISI 8740 steel, is 976.3 mm in length with a maximum diameter of 383 mm. The two bells, internally toothed, rest on the hubs and are connected together by a sleeve collar; two metal O-rings, pressure mounted in circumference slots cut into the

teeth of the bell, allow the bell-cylinder system an axial slip of 6 mm. The hubs, toothed externally with 88 teeth, are keyed on the turbine and compressor shafts; two keys and two threaded locking rings prevent, respectively, tangential and axial movement. The smaller longitudinal dimensions of the hub teeth compared to those of the bells, combined with radial and tangential gap, allow the shafts to become misaligned. A gas balancing system, which uses a disk keyed to the shaft, makes it possible to limit the axial thrust and the vibrations. To prevent excessive vibrations from damaging the seals, during operation a control system verifies that radial movement at the bearings never exceeds the allowed tolerances ( $0.24 \div 0.28 \text{ mm}$  for the compressor bearings and  $0.3 \div 0.358 \text{ mm}$  for the turbine bearings).

### III. NUMERICAL MODEL

The numerical model was developed using: the ADAMS calculation programme to construct the multibody model of the turbo-compressor; and the MSC/NASTRAN calculation programme which, through modal analysis of the components, was used to generate transfer files simulating the flexible behaviour of the parts in the multibody code [13], [14]. The approach followed in order to consider the bodies flexible was the modal approach developed by Craig and Bampton [15], which allows the number of generalised coordinates to be reduced to a minimum and offers greater freedom in the definition of the constraint conditions at the boundary points.

The transfer file contains the stiffness and damping matrices of dimensions  $(6N \times 6N)$ , where  $N$  is the number of points used in modelling the flexible parts; five for the turbine, two for the coupling and twelve for the compressor. A characteristic aspect of this modelling is the use of kinetic reference systems, KRF (Kinematic Reference Frame), integral with each rigid part making up the discretized flexible body. In this approach, each substructure of the FEM is represented by a superelement characterised by the above stiffness and damping matrices [16]. The movements of each substructure are calculated locally with respect to the corresponding KRF; the overall elastic deformation of the flexible body is obtained from the set of single movements of the rigid parts into which it is discretized. The definition of the matrix of concentrated mass is obtained through the localisation of a centre of mass for each part, with the inertial properties referring to it. The mass of each part is independent of the rest of the system, so that the extra-diagonal terms are eliminated from the mass matrix. On the basis of the blueprints supplied by MAAG and using digital photogrammetry acquisition as described in [17], [18], CAD 3D geometries were developed for the following parts: the compressor shaft; the turbine shaft; the six rotors; the thrust equaliser; the Kingsbury rings of the thrust bearings; all the parts of the diffusers of the keyed stages in the rotor; the threaded locking rings which axially constrain the rotors and diffusers; the hubs of the toothed coupling keyed to the stator and the locking rings which constrain them axially (Fig. 1).

The construction of the finite element model required a simplification of these geometries, eliminating some features

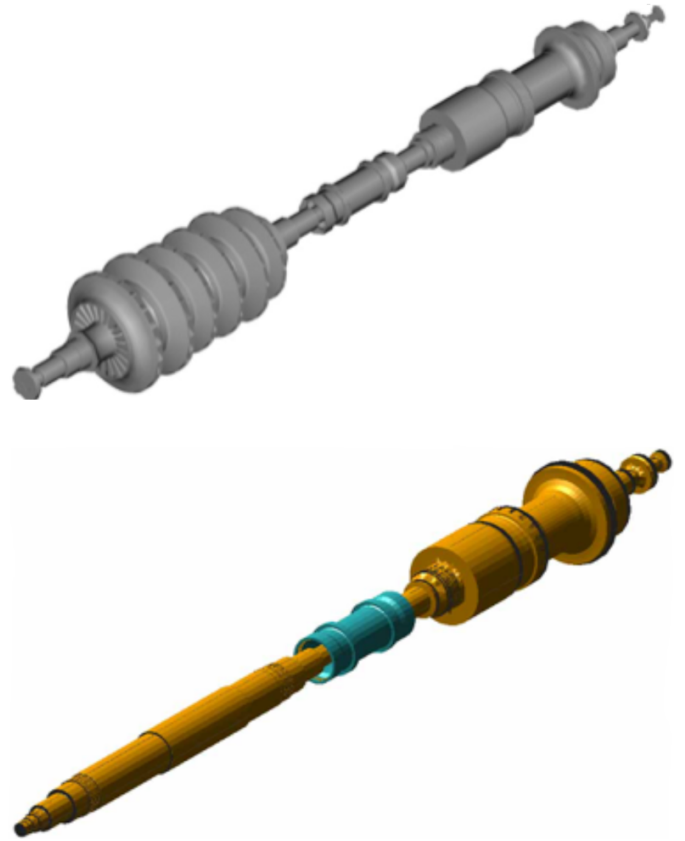


Fig. 1. 3D parametric model (top); flexible multibody elements (top).

TABLE II. ELEMENTS IN FE MODELS

	Elements	Nodes	Typology
Turbine	22567	5620	Tet 4
Coupling	6638	13427	Tet 10
Compressor	13921	28186	Tet 10

irrelevant to the dynamic behaviour. The number of hexahedral elements and nodes are reported in Table II.

### IV. HYDRODYNAMIC BEARINGS

Particular attention was paid to the modelling of the hydrodynamic bearings, on which the dynamic stability of the system depends.

For each shaft, three-component forces were applied at the mid-line of each bearing: the two radial components  $x$  and  $z$  (Fig. 2) reproduce the hydrodynamic reaction of the bearing on the journal, while the  $y$  component, using a bistop function, simulates the thrust bearing [19], [20], [21].

Integrating the differential equations of Reynolds, in accordance with the Ocvirk and Dubois approximation for short bearings, the characteristics of the lubrication fluid in the bearings were obtained (eqq. 1-7) which determine, together

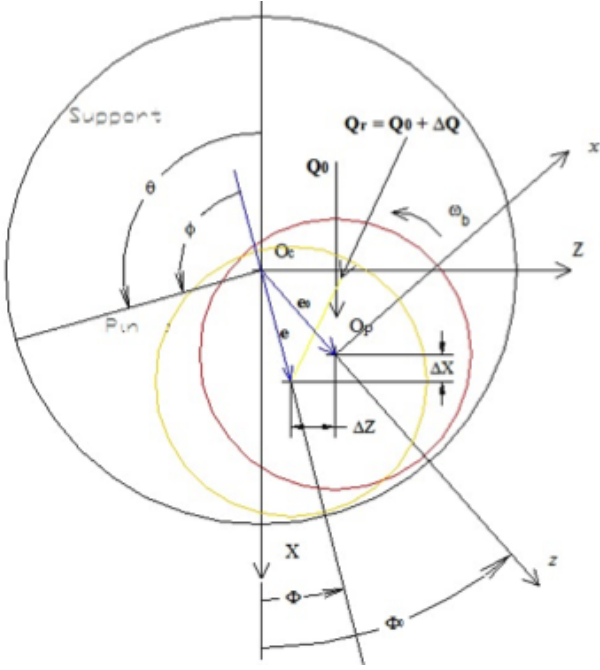


Fig. 2. Transversal cross-section of the bearing.

with the static component of the load, the elastohydrodynamic reaction of the bearing on the pivot (eq. 8).

$$k_{XY} = \frac{\eta_0 \omega_b r_b b^3 \varepsilon_0}{c^3} \left[ \frac{\sin^2 \Phi_0}{(1 - \varepsilon_0^2)^2} + \frac{3 \pi \varepsilon_0 \cos \Phi_0 \sin \Phi_0}{4(1 - \varepsilon_0^2)^{\frac{5}{2}}} + \frac{2(1 + \varepsilon_0^2) \cos^2 \Phi_0}{(1 - \varepsilon_0^2)^3} \right] \quad (1)$$

$$k_{XZ} = \frac{\eta_0 \omega_b r_b b^3}{c^3} \left[ \frac{\pi(1 + 2\varepsilon_0^2) \sin^2 \Phi_0}{4(1 - \varepsilon_0^2)^{\frac{5}{2}}} + \frac{\varepsilon_0(1 + 3\varepsilon_0^2) \cos \Phi_0 \sin \Phi_0}{(1 - \varepsilon_0^2)^3} + \frac{\pi \cos^2 \Phi_0}{4(1 - \varepsilon_0^2)^{\frac{3}{2}}} \right] \quad (2)$$

$$k_{YZ} = \frac{\eta_0 \omega_b r_b b^3}{c^3} \left[ -\frac{\pi \sin^2 \Phi_0}{4(1 - \varepsilon_0^2)^{\frac{3}{2}}} + \frac{\varepsilon_0(1 + 3\varepsilon_0^2) \cos \Phi_0 \sin \Phi_0}{(1 - \varepsilon_0^2)^3} - \frac{\pi(1 + 2\varepsilon_0^2) \cos^2 \Phi_0}{4(1 - \varepsilon_0^2)^{\frac{5}{2}}} \right] \quad (3)$$

$$k_{ZZ} = \frac{\eta_0 \omega_b r_b b^3 \varepsilon_0}{c^3} \left[ \frac{2(1 + \varepsilon_0^2) \sin^2 \Phi_0}{(1 - \varepsilon_0^2)^3} + \frac{3 \pi \varepsilon_0 \cos \Phi_0 \sin \Phi_0}{4(1 - \varepsilon_0^2)^{\frac{5}{2}}} + \frac{\cos^2 \Phi_0}{(1 - \varepsilon_0^2)^2} \right] \quad (4)$$

$$r_{XX} = \frac{\eta_0 r_b b^3}{c^3} \left[ \frac{\pi \sin^2 \Phi_0}{2(1 - \varepsilon_0^2)^{\frac{3}{2}}} + \frac{4 \varepsilon_0 \cos \Phi_0 \sin \Phi_0}{(1 - \varepsilon_0^2)^2} + \frac{\pi(1 + 2\varepsilon_0^2) \cos^2 \Phi_0}{(1 - \varepsilon_0^2)^{\frac{5}{2}}} \right] \quad (5)$$

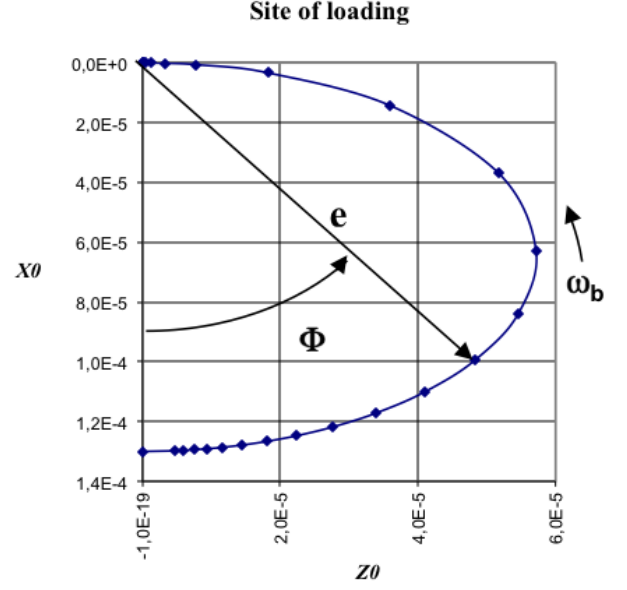


Fig. 3. Bearing site of loading.

$$r_{XZ} = r_{ZX} = \frac{\eta_0 r_b b^3 \varepsilon_0}{c^3} \left[ -\frac{4 \sin^2 \Phi_0}{(1 - \varepsilon_0^2)^2} + \frac{3 \pi \varepsilon_0 \cos \Phi_0 \sin \Phi_0}{2(1 - \varepsilon_0^2)^{\frac{5}{2}}} - \frac{\cos^2 \Phi_0}{2(1 - \varepsilon_0^2)^2} \right] \quad (6)$$

$$r_{ZZ} = \frac{\eta_0 r_b b^3}{c^3} \left[ \frac{\pi(1 + 2\varepsilon_0^2) \sin^2 \Phi_0}{2(1 - \varepsilon_0^2)^{\frac{5}{2}}} + \frac{4 \varepsilon_0 \cos \Phi_0 \sin \Phi_0}{(1 - \varepsilon_0^2)^2} + \frac{\pi^2 \Phi_0}{2(1 - \varepsilon_0^2)^{\frac{3}{2}}} \right] \quad (7)$$

$$\begin{bmatrix} F_X(t) \\ F_X(t) \end{bmatrix} = \begin{bmatrix} F_X(X_0, Z_0, 0, 0) \\ 0 \end{bmatrix} + \begin{bmatrix} k_{XX} & k_{XZ} \\ k_{ZX} & k_{ZZ} \end{bmatrix} \begin{bmatrix} (X - X_0) \\ (Z - Z_0) \end{bmatrix} - \begin{bmatrix} r_{XX} & r_{XZ} \\ r_{ZX} & r_{ZZ} \end{bmatrix} \begin{bmatrix} \dot{X} \\ \dot{Z} \end{bmatrix} \quad (8)$$

The static components of the load, determined at each equilibrium configuration  $(X_0, Y_0)$ , on varying the velocity, are shown in Fig. 3, while the static reactions of the bearings are reported in Tab. III.

## V. CONTACT BETWEEN THE TEETH

Three-component vector forces were used to model the forces exchanged between the teeth of the hubs and those of the bells. Using IMPACT and BISTOP functions, these vector forces limit the axial, radial and tangential movements of the hubs inside the bells.

The axial movement of the sleeve collar-bells system ( $\pm 3 \text{ mm}$ ) is limited by the z components of the forces of contact between the teeth simulating the behaviour of the two

TABLE III. LOAD ON THE BEARINGS ( $F_{MAG}$ )

Bearings	Load [N]
Compressor external side	15433
Compressor coupling side	18964
Turbine coupling side	17980
Turbine external side	17840

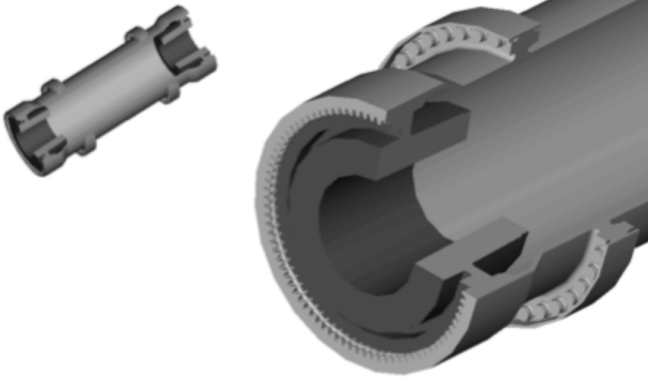


Fig. 4. Detail of the coupling.

O-rings pressure mounted inside the bells. The x component of the vector force is applied to the tooth flank in the tangential direction, while the y component is applied in the radial direction (Fig. 4 and Fig. 5).

## VI. MODEL VALIDATION AND ANALYSIS OF RESULTS

The model, was validated on the basis of experimental measurements conducted at the Enichem Priolo plant using inductive proximity transducers, which measure the radial and axial movements of the shafts in their bearings. The experimental measurements of the monitoring system were filtered and only those frequencies of major interest appear in the spectra, i.e. frequencies up to the value at the speed of rotation and at multiples of this speed [22], [23]. For comparison, figure 6 shows the frequency spectra of the movements measured in the turbine bearing near the coupling. In correspondence with the first harmonic (65.3 Hz) the amplitude values are almost coincident for both the numerical model and the experimental measurements. The further close agreement between values for the subsequent harmonics confirms that the behaviour of the numerical model is very close to that of the real system.

The numerical modal analysis was performed using the Lanczos method of constants.

Since the frequency corresponding to maximum speed (4000 rpm) is 66 Hz, the possibility of torsional resonance with the two shafts and the coupling is improbable and, therefore, the operating anomalies are considered to be the result of shaft misalignment. Thus, as well as an analysis of the dynamic behaviour of the system under normal operating conditions, a misalignment between the shafts was simulated with values of

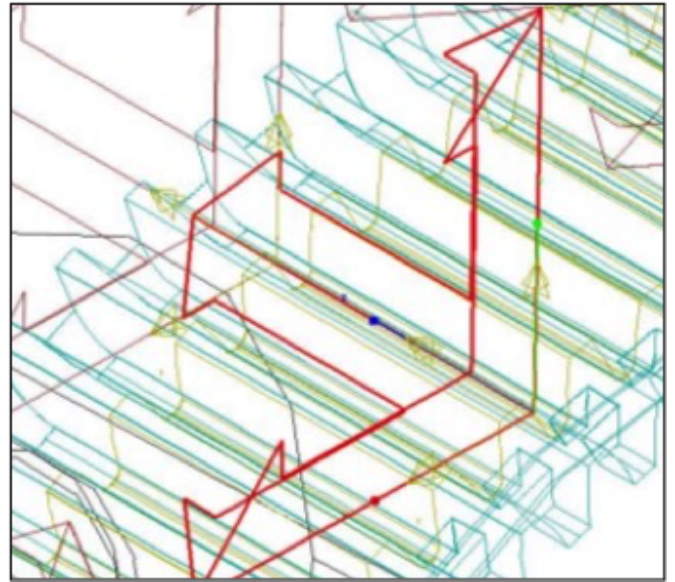


Fig. 5. Contact force between teeth.

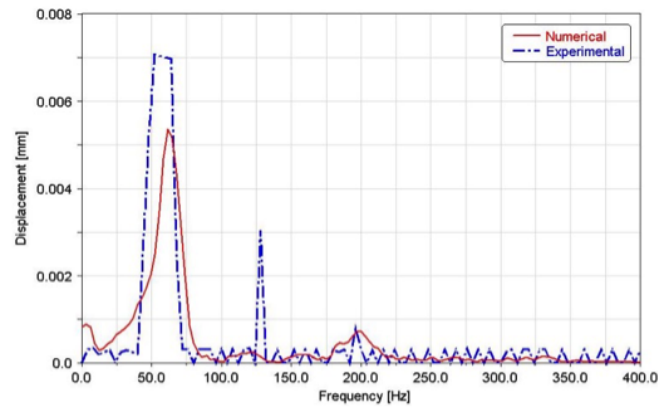


Fig. 6. Frequency spectrum of the movements in the internal turbine bearing.

4' and 9', the maximum values admitted by the manufacturer at speed and in transient, respectively.

### A. Normal operation

Fig. 7 shows the displacement calculated during six revolutions at a speed of 3920 rpm at the two sensors mounted at  $\pm 45^\circ$  with respect to the vertical, in the turbine bearing located near the coupling.

The displacements, calculated under normal operating conditions, have amplitudes of less than 1.5 mils (0.0381 mm) and in the real system can, therefore, be considered background noise produced by the surface roughness of the pivot. The coincidence of the values measured by two sensors indicates that the pivot rotates with an almost constant eccentricity. The values of the displacements for rigid and deformable elements are compared in Fig. 8.

The need to use a model with deformable elements appears evident. Although this model presents considerable difficulty in construction and longer calculation times, it yields results

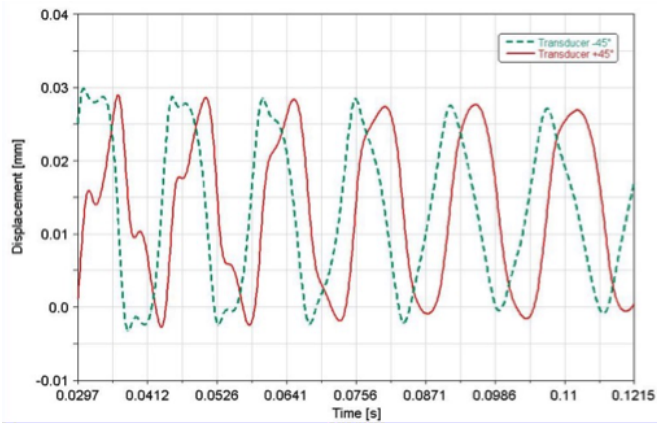


Fig. 7. Displacements in the turbine bearing (coupling side).

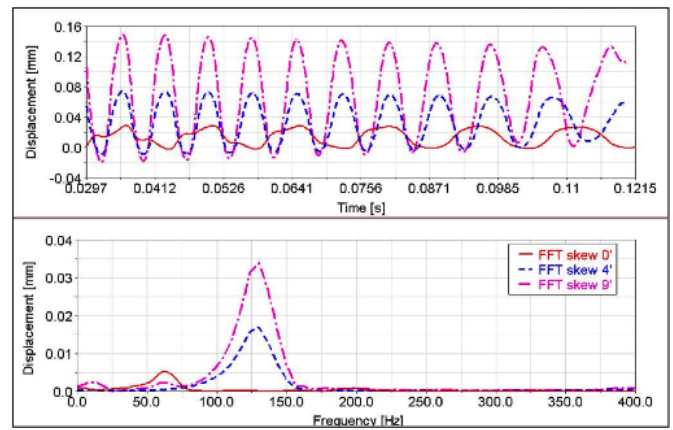


Fig. 9. Vibrations in the turbine bearing with misalignments.

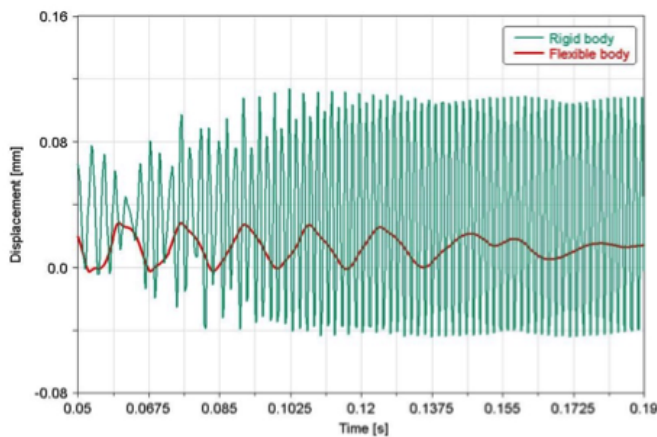


Fig. 8. Comparison of displacements in the turbine bearing, rigid and deformable shafts.

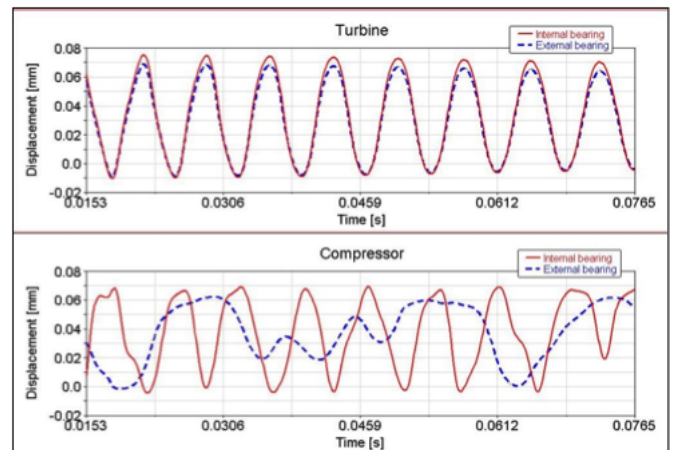


Fig. 10. Comparison of displacements in the internal and external bearings.

which are comparable to those measured experimentally. In the model with rigid elements, instead, the displacement values are incompatible with the normal operation of the machine, above all considering the fact that they were calculated with zero misalignment.

### B. Misalignment of the shafts

Fig. 9 shows a comparison of the displacements and relative spectra of the turbine bearing at the sensor at  $+45^\circ$  for misalignments of zero,  $4'$  and  $9'$ . A misalignment of  $4'$  leads to displacements of about 3 mils (0.0762 mm), the limiting value beyond which the critical operation alarm is activated. A misalignment of  $9'$  produces displacements of almost 6 mils (0.1524 mm) which result in the machine blocking, given that this exceeds the maximum allowed radial play of 0.13 mm. The frequency diagrams evidence that increasing the misalignment results in a decrease in the amplitude of the vibrations at 3920 rpm (65.3 Hz) and conversely, a considerable increase at double the rotation speed. Comparing these data with those of Fig. 4, it can be deduced that during the experimental measurements the machine was operating with a misalignment of less than  $4'$ . The misalignments, therefore,

provoke vibrations at frequencies which are multiples of the frequency at operating speed.

Finally, Fig. 10 shows a comparison of the displacements calculated in the two bearings (internal and external with respect to the coupling) of the compressor and turbine, when a misalignment of  $4'$  is simulated. In the turbine, the values of the displacements are substantially coincident and show a fairly regular trend due to the fact that jibbing between the turbine itself and the coupling was provoked to simulate the misalignment. In the compressor, the internal bearing shows a trend similar to that of the turbine, while the external bearing shows a rather irregular trend as a result of being dragged by the coupling and thus oscillating around the equilibrium position.

### C. Energy of deformation

The possibility of constructing a reliable numerical bearing model with flexible bodies able to simulate the dynamic behaviour of the turbo-compressor in a realistic manner also made it possible to obtain complete information regarding the stress and strain states of the various machine components while operating. In particular it was possible to analyse the impulsive interactions between the teeth of the hubs and those of the bells

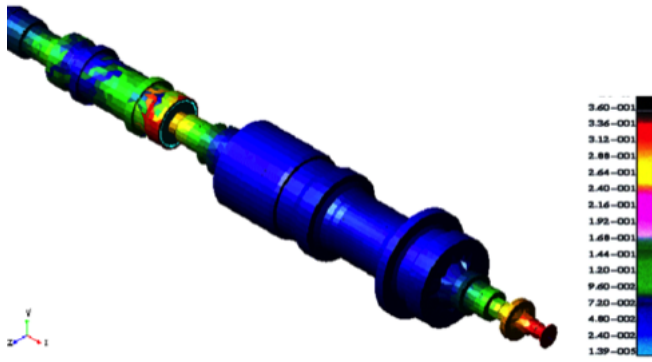


Fig. 11. Strains in the coupling and bearings (misalignment of  $9'$  with jibbing).

when jibbing occurs, evaluating the stress and strain states. The simulations of misalignment with jibbing between the axis of the turbine and that of the coupling reproduce the most severe operating conditions; the bells present elevated strains (Fig. 9) accompanied by a displacement of the centres of rotation of the pivots in their bearings. The stress peaks are concentrated on the external surface of the bells and at the toothing, reaching stresses close to the elastic limit (0.21 GPa).

Figure 9 shows the strain distributions in the zones of the bells and in the bearings where the stresses reach maximum values, remaining, however, below the elastic limit. From the analysis of the dynamic behaviour of the turbo-compressor, it emerged that in misalignments of up to  $9'$ , the strains in the bells and bearings in any case allow the machine to operate; the limits of vibration anticipated for the pivots are not exceeded and the lubrication film in the bearings is not ruptured. During the simulations of jibbing, it was possible to distinguish two phases; in the first phase a considerable amount of energy is absorbed by the bells, followed by a phase of settling in which the shafts find a new position of dynamic equilibrium on the bearings and the strain energy of the bells decreases.

## VII. CONCLUSIONS

The dynamic optimization of a turbo-compressor, simulated through a complete model with flexible bodies which reproduced all the interactions between the parts of the system was performed. The validity of the model was verified through the comparison of data obtained by calculation with that measured experimentally provided by ENICHEM. The models usefulness is demonstrated by making it possible to study typical situations of malfunction of the real system, such as the jibbing of the toothed coupling, the most frequent cause of alarms signalled by the vibration monitoring system. The study allowed the simulation of the functioning of the rotors at operating speed, performing an investigation into the maximum permitted misalignment between the shafts and the coupling. It was possible to verify the entity of the displacements of the bearing pivots, and analyse the strains and the stress states in the toothed bells of the turbine-compressor coupling.

Through the exact determination of the natural frequencies of the three main components of the system, it was possible to affirm that the critical operating characteristics are not linked to phenomena of resonance produced by applied forces originating in the bearings.

## ACKNOWLEDGMENT

This study was made possible by the helpfulness of Enichem Priolo. The authors wish to thank Engineer Antonio Rosolia, who supplied the data and material necessary for the development of this research.

## REFERENCES

- [1] W. Jiang and T. C. Lim, "Spectral-based direct multi-substructure analysis of mechanical system vibration response," *Noise Control Engineering Journal*, vol. 63, no. 2, pp. 117–137, 2015.
- [2] F. Fumei, L. Ping, and W. Gengshen, "Experimental research on steam-turbine rotor vibration fault diagnosis based on the fractal box counting dimension," *Nuclear Power Engineering*, vol. 27, no. 1, pp. 85–89, 2006.
- [3] A. Zile, D. Taradai, S. Tomashevskii, and Y. A. Shuranova, "Studying the torsional vibrations of turbine shaft trains," *Power Technology and Engineering*, vol. 47, no. 6, pp. 470–477, 2014.
- [4] M. Cali, G. Sequenzia, S. Oliveri, and G. Fatuzzo, "Meshing angles evaluation of silent chain drive by numerical analysis and experimental test," *Meccanica*, vol. 51, no. 3, pp. 475–489, 2016.
- [5] E. Pedullà, F. Lo Savio, S. Boninelli, G. Plotino, N. Grande, E. Rapisarda, and G. La Rosa, "Influence of cyclic torsional preloading on cyclic fatigue resistance of nickel–titanium instruments," *International endodontic journal*, vol. 48, no. 11, pp. 1043–1050, 2015.
- [6] E. Pedulla, F. L. Savio, G. Plotino, N. M. Grande, S. Rapisarda, G. Gambarini, and G. La Rosa, "Effect of cyclic torsional preloading on cyclic fatigue resistance of protaper next and mtwo nickel–titanium instruments," *Giornale Italiano di Endodonzia*, vol. 29, no. 1, pp. 3–8, 2015.
- [7] E. Pedullà, F. L. Savio, S. Boninelli, G. Plotino, N. M. Grande, G. La Rosa, and E. Rapisarda, "Torsional and cyclic fatigue resistance of a new nickel–titanium instrument manufactured by electrical discharge machining," *Journal of endodontics*, vol. 42, no. 1, pp. 156–159, 2016.
- [8] N. Bachschmid, G. Salvini, E. Tanzi, and E. Pesatori, "The influence of blade row dynamics on lateral and torsional shaft vibrations in steam turbines," in *Proceedings of the 9th IFToMM International Conference on Rotor Dynamics*. Springer, 2015, pp. 113–127.
- [9] S. Brusca, R. Lanzafame, A. Marino Cugno Garrano, and M. Messina, "Dynamic analysis of combustion turbine running on synthesis gas," *International Journal of Applied Engineering Research*, vol. 10, no. 21, pp. 42 244–42 253, 2015.
- [10] G. Sequenzia, S. Oliveri, G. Fatuzzo, and M. Cali, "An advanced multi-body model for evaluating riders influence on motorcycle dynamics," *Proceedings of the Institution of Mechanical Engineers, Part K: Journal of Multi-body Dynamics*, vol. 229, no. 2, pp. 193–207, 2015.
- [11] M. Cali, S. M. Oliveri, G. Sequenzia, and G. Fatuzzo, "An effective model for the sliding contact forces in a multibody environment," in *Advances on Mechanics, Design Engineering and Manufacturing*. Springer, 2017, pp. 675–685.
- [12] G. Dubois, F. W. Ocvirk, and R. Wehe, *Study of effect of a non-newtonian oil on friction and eccentricity ratio of a plain journal bearing*. National Aeronautics and Space Administration, 1960, vol. 427.
- [13] G. Sequenzia, S. Oliveri, M. Calabretta, G. Fatuzzo, and M. Cali, "A new methodology for calculating and modelling non-linear springs in the valve train of internal combustion engines," SAE Technical Paper, Tech. Rep., 2011.
- [14] G. Sequenzia, S. Oliveri, and M. Cali, "Experimental methodology for the tappet characterization of timing system in ice," *Meccanica*, vol. 48, no. 3, pp. 753–764, 2013.
- [15] M. Géradin and A. Cardona, *Flexible multibody dynamics: a finite element approach*. Wiley, 2001.

- [16] F. Bonanno, G. Capizzi, S. Coco, A. Laudani, and G. L. Sciuto, "A coupled design optimization methodology for li-ion batteries in electric vehicle applications based on fem and neural networks," in *2014 International Symposium on Power Electronics, Electrical Drives, Automation and Motion*, June 2014, pp. 146–153.
- [17] M. Cali, D. Speranza, and M. Martorelli, "Dynamic spinnaker performance through digital photogrammetry, numerical analysis and experimental tests," in *Advances on Mechanics, Design Engineering and Manufacturing*. Springer, 2017, pp. 585–595.
- [18] M. Cali and F. L. Savio, "Accurate 3d reconstruction of a rubber membrane inflated during a bulge test to evaluate anisotropy," in *Advances on Mechanics, Design Engineering and Manufacturing*. Springer, 2017, pp. 1221–1231.
- [19] B. J. Hamrock, S. R. Schmid, and B. O. Jacobson, *Fundamentals of fluid film lubrication*. CRC press, 2004.
- [20] Y. Cui, Y. Wang, and J. Zhong, "Numerical analysis on the nonlinear hysteresis phenomenon associated with instability of a steam turbine rotor-bearing system," in *Proceedings of the 9th IFToMM International Conference on Rotor Dynamics*. Springer, 2015, pp. 2071–2081.
- [21] E. Zanetti, S. Musso, and A. Audenino, "Thermoelastic stress analysis by means of a standard thermocamera," *Experimental Techniques*, vol. 31, no. 2, pp. 42–50, 2007.
- [22] F. Bonanno, G. Capizzi, G. L. Sciuto, D. Gotleyb, S. Linde, and R. Shikler, "Extraction parameters and optimization in organic solar cell by solving transcendental equations in circuital models combined with a neuroprocessing-based procedure," in *2016 International Symposium on Power Electronics, Electrical Drives, Automation and Motion (SPEEDAM)*, June 2016, pp. 872–877.
- [23] F. Bonanno, G. Capizzi, and G. L. Sciuto, "A neuro wavelet-based approach for short-term load forecasting in integrated generation systems," in *2013 International Conference on Clean Electrical Power (ICCEP)*, June 2013, pp. 772–776.